A benchmark study of dioxygen complexes based on coupled cluster and density functional theory

Marcel Swart,[a,b,*] and Marc Reimann[c]

a) ICREA, Pg. Lluís Companys 23, 08010 Barcelona, Spain

b) IQCC and Dept. Chem., Univ. Girona, c/M.A. Capmany 69, 17003 Girona, Spain

c) Institut für Chemie, Theoretische Chemie/Quantenchemie, Technische Universität Berlin, Sekr. C7, Straße des 17. Juni 135, D-10623 Berlin, Germany

marcel.swart@icrea.cat

Abstract

A set of five compounds containing peroxo, superoxo or bis-μ-oxo moieties has been studied in the gas phase using CCSD(T)/aug-cc-pVQZ, also in combination with Goodson's continued fraction approach. The corresponding analytical frequencies corroborate assignments of bands from experiments, and thus provide a consistent set of reference data that can be used for benchmarking a range of density functional approximations. A total of 100 density functionals have been checked for the general bond lengths, the specific peroxo/superoxo bond lengths, angles, vibrational frequencies and electronic energies. There is not one density functional that performs equally well for all of these properties, not even within one class of density functionals.

Keywords

Density functional theory – Coupled cluster – Computational chemistry – Dioxygen compounds.

Introduction

Dioxygen can coordinate to first-row transition metals (in different oxidation and spin states) with several protonation states, and hapticity, leading to e.g. peroxo, superoxo, hydroperoxo or bis-μ-oxo species (see Scheme 1). Although crystal structures exist for all of these species,[1,2] the

corresponding complexes are too large for treatment by accurate wavefunction methods like CCSD(T) with large basis sets (aug-cc-pVQZ or better). This prevents the systematic validation[3–8] of more efficient yet less accurate quantum-chemistry methods, e.g. based on density functional theory,[9] leading to uncertainty about the reliability and appropriateness of different density functionals[10,11] for this metal-dioxygen chemistry.

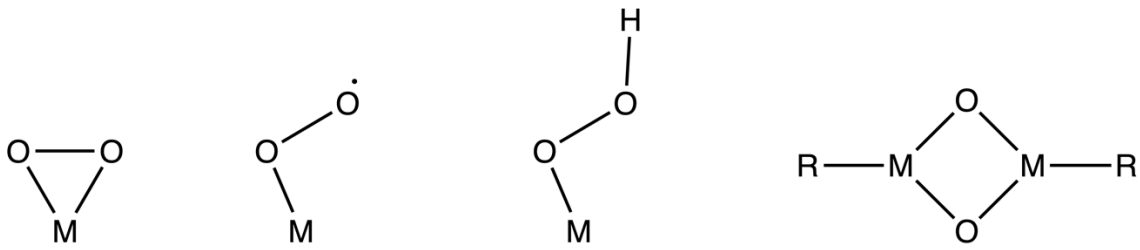

Scheme 1. Typical coordination of dioxygen towards (transition-)metal centers

Fortunately, in the early 2000s a series of papers by Schnöckel[12,13] and co-workers reported the detection of peroxo and bis-μ-oxo complexes of aluminium (see Scheme 2), with vibrational spectroscopic data available for characterization. Furthermore, Tremblay and Roy characterized silicon trioxide compounds spectroscopically.[14] Since these complexes are small (maximum six atoms), and highly symmetric, it is possible to study them by high-level wavefunction methods with sufficiently large basis sets. Hence, here we used CCSD(T)[15] with the aug-cc-pVQZ (and aug-cc-pV(X+d)Z,[16] X=T,Q) basis sets for complexes **1**-**5** (Scheme 2) to optimize their structure and compute the corresponding vibrational frequencies. Because of the well-known instability of coupled cluster frequencies for close-lying electronic states, in particular when using unrestricted Hartree-Fock (HF) orbitals,[17] we have complemented these data with CCSD(T) results based on restricted open-shell Kohn-Sham (ROKS) PBE orbitals, and CASPT2 frequencies. These results match the standard CCSD(T) results very well, when the underlying HF solution exhibits no close-

lying electronic states. These data can then serve as reference data for the development of new density functionals. Here, the results were used as reference data for the benchmarking of density functional approximations, to explore how well the latter reproduce the metal-O and O-O distances, the angles, the vibrational frequencies, and the corresponding electronic energies.

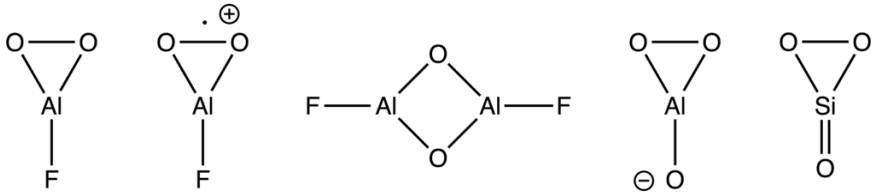

Scheme 2. Al/Si complexes studied in this paper (complex **2** has overall charge +1, complex **4** overall charge -1, the other three are charge neutral). Experimental vibrational spectra are available for **1**,[12] **3**,[13] and for **5**.[14]

Results and discussion

Coupled cluster results. The experimentally observed vibrational data[12–14] for **1**, **3**, **5** are reported in Table 1, together with the CCSD(T)/aug-cc-pVQZ values. Also included are two related compounds, **2** and **4**, for which only the coupled cluster data are available. For **1** and **2** we also report CASPT2 results based on a CASSCF(14,8) reference. In general, there is a very good agreement between the experimentally observed peaks and the coupled cluster data. For instance, for $[FAlO_2]^0$ the peaks were observed experimentally at 1077 and 782 cm^{-1}, which match the harmonic coupled cluster frequencies of 1102 and 797 cm^{-1}; note that the difference between experiment and theory (2-3%) is due to anharmonicity. We have computed the anharmonic CCSD(T) frequencies based on VPT2, which shows a very good match of the effect of anharmonicity on these frequencies (see Table 2). The only exception perhaps may be the 1015 cm^{-1} band of **3**, which after anharmonic corrections is observed at 995 cm^{-1} with CCSD(T).

Few of the computed frequencies were observed experimentally, either due to too low intensity or not being able to assign these specifically to one of the manifolds of possible compounds that might be present in the experiments. For instance, in the reaction of AlF with O_2 the authors observed (at least) three species: **1**, **3** and a third one involving four oxygens (assigned[12] as a di-superoxo species $[FAl(O_2^{\bullet -})_2]^0$). Based on isotope effects when treating all species with either $^{16}O_2$, $^{18}O_2$ or a mixture of these, they were able to assign most of the observed peaks to one of these three species.

Table 1. Vibrational data (cm^{-1}) for dioxygen complexes[a] (harmonic frequencies for CCSD(T))

1		**2**	**3**		**4**	**5**	
exp.[b]	CCSD(T)[c]	CCSD(T)[d]	exp.[e]	CCSD(T)[c]	CCSD(T)[c]	exp.[f]	CCSD(T)[c]
1077.3	1102.3 (160.6)	1111.0	1015.0	1014.5 (0.0)	1100.4 (82.8)	1363.5	1382.2 (121.2)
781.8	797.1 (26.7)	1001.4	942.8	966.1 (544.4)	748.1 (25.5)	877.1	887.6 (5.0)
-	720.5 (8.8)	609.8	812.9	821.4 (312.4)	673.3 (27.2)	855.3	860.4 (17.5)
-	476.0 (13.0)	596.1	-	749.3 (0.0)	544.0 (51.0)	-	511.3 (16.9)
-	228.5 (122.1)	173.2	-	690.5 (0.0)	270.1 (33.2)	292.0	307.2 (80.7)
-	219.8 (71.5)	172.8	-	665.1 (32.1)	256.8 (11.9)	287.8	296.4 (53.0)
			-	404.5 (0.0)			
			-	400.7 (184.6)			
			-	243.7 (0.0)			
			-	225.2 (0.0)			
			-	171.1 (30.5)			
			-	94.5 (12.6)			

a) shown in (parentheses) are the computed IR intensities ($km \cdot mol^{-1}$); b) ref. [12]; c) CCSD(T)/aug-cc-pVQZ; d) ROKS-CCSD(T)/aug-cc-pVQZ on PBE orbitals; e) ref. [13]; f) ref. [14]

The normal modes for $[FAlO_2]^0$ from CCSD(T)/aug-cc-pVQZ consist of an Al-F stretch at 1102 cm^{-1}, the anti-symmetric (797 cm^{-1}) and symmetric (721 cm^{-1}) Al-O_2 vibrations, the O-O vibration (476 cm^{-1}) and the out-of-plane (δ-oop, 229 cm^{-1}) and in-plane (δ-ip, 220 cm^{-1}) δ(FAlOO) distortion. Similar modes are found for $[OAlO_2]^0$: ν(Al-O) 1100 cm^{-1}, ν_{sym}(Al-O_2) 748 cm^{-1}, ν_{asym}(Al-O_2) 673 cm^{-1}, ν(O-O) 544 cm^{-1}, ν(δ-oop) 270 cm^{-1}, ν(δ-ip) 257 cm^{-1}, and for $[OSi(O_2)]^0$: ν(Si-O) 1382 cm^{-1}, ν_{sym}(Si-O_2) 888 cm^{-1}, ν_{asym}(Si-O_2) 860 cm^{-1}, ν(O-O) 511 cm^{-1}, ν(δ-oop) 307 cm^{-1}, ν(δ-ip) 296 cm^{-1}. Note that in these latter cases the symmetric Al/Si-O_2 stretch shows a higher

frequency than the asymmetric stretch, unlike the case of $[FAlO_2]^0$. Instead, for $^2[FAlO_2]^{\bullet+}$ the normal modes are shifted drastically in some cases: ν(Al-F) 1111 cm^{-1}, ν(O-O)$^\bullet$ 1001 cm^{-1}, ν_{sym}(Al-$O_2^\bullet$) 610 cm^{-1}, ν_{asym}(Al-$O_2^\bullet$) 596 cm^{-1}, ν(δ-oop) 173 cm^{-1}, ν(δ-ip) 173 cm^{-1}. These calculations, however, had to be performed using PBE-based orbitals, as the usage of HF based orbitals resulted in unphysically large shifts. This approach is well suited as it introduces only marginal deviations from HF-based results for all other species (see Table S7). Finally, for $[FAl(\mu\text{-}O)_2AlF]^0$ the Al-F stretches are found at 1015 cm^{-1} (sym) and 966 cm^{-1} (asym), the Al-O_2-Al stretches at 691 cm^{-1} (asym) and 665 cm^{-1} (sym), and further modes involving the diamond-core breathing mode (749 cm^{-1}), FAl-AlF stretch (405 cm^{-1}), in-plane Al_2 vs. O_2 (821 cm^{-1}), out-of-plane Al_2 vs. O_2 (401 cm^{-1}), rocking (244 cm^{-1}) vs. flying (171 cm^{-1}) vs. out-of-plane (95 cm^{-1}) motions of Al_2O_2 vs. F_2, and the anti-symmetric out-of-plane wobble of Al_2F_2 (225 cm^{-1}). Note that gif-movie files for all modes are available in Supporting Information.

Table 2. Effect of anharmonicity on computed vibrational data (cm^{-1}) for dioxygen complexes[a]

1			**3**			**5**		
exp.[b]	harm.	anharm.	exp.[c]	harm.	anharm.	exp.[d]	harm.	anharm.
1077.3	1093.7	1078.3	1015.0	1007.0	994.7	1363.5	1384.7	1364.4
781.8	790.9	781.2	942.8	958.1	943.8	877.1	890.1	877.9
-	716.6	707.3	812.9	816.9	805.9	855.3	863.3	851.9
-	476.8	463.1	-	747.0	738.5	-	513.1	496.1
-	232.8	233.0	-	684.9	673.2	292.0	304.5	303.4
-	219.3	219.5	-	660.2	657.1	287.8	296.5	295.1
				404.5	399.7			
				399.9	397.6			
				245.8	245.2			
				229.4	229.5			
				173.7	173.7			
				98.1	98.3			

a) data obtained at CCSD(T)/def2-tzvpd; b) ref. [12]; c) ref. [13]; d) ref. [14]

The geometric variables (bonds, angles) from the coupled cluster calculations are reported in Table 3. Based on the revised covalent radii by Alvarez and co-workers from 2008,[18] one would expect Al-F bonds of 1.78 Å, Al-O bonds of 1.87 Å, and Si-O bonds of 1.77 Å. Here, we observe Al-F, Al-O and Si-O bonds that are significantly shorter (0.15-0.20 Å). However, they are consistent with previous computational studies at lower levels of theory.[13,19,20] Furthermore, the coupled cluster method with such a large basis set is often considered the 'gold standard' of computational chemistry. Indeed, the strong coherence between the computed and observed IR frequencies reinforce this notion. For this reason, the coupled cluster data provide a good reference set to be able to compare density functional approximations with.

Table 3. Geometric variables obtained at CCSD(T)/aug-cc-pVQZ (using ROKS orbitals for **2**)

bond	(Å)	angle	(°)
1			
F-Al	1.62978	F-Al-O	150.286
Al-O(O_2)	1.69710	O-Al-O[a]	59.428
O-O	1.68239		
2			
F-Al	1.59705	F-Al-O	156.951
Al-O(O_2)	1.78213	O-Al-O[a]	46.098
O-O	1.39549		
3			
F-Al	1.63660	F-Al-O	133.328
Al-O	1.73798	Al-O-Al	86.655
Al-Al[a]	2.38510		
4			
O-Al	1.63751	O-Al-O	152.282
Al-O(O_2)	1.74850	O-Al-O[a]	55.437
O-O	1.62655		
5			
O-Si	1.50991	O-Si-O(O_2)	148.864

Si-O(O_2)	1.62299	O(O_2)-Si-O(O_2)[a]	62.271
O-O	1.67839		

a) not used for the deviations of density functional results (use of symmetry makes this value dependent on the other angle)

Density functional results. A total of 100 density functional approximations (DFAs) were tested against the coupled cluster reference data. Note that the same conditions were used as were employed for coupled cluster: using the aug-cc-pVQZ basis in the gas phase and without relativistic corrections. Hence, we looked at the bond lengths and angles (see Table 3), frequencies, and difference with the electronic energy of Goodson's approach.[21] Clearly, the latter check is merely informative, since DFT and coupled cluster approach the solution of the Schrödinger equation in a different manner. Density functional approaches modify the Hamiltonian, while the coupled cluster calculations improve the wavefunction within Schrödinger's equation. We also note that the standard CCSD(T) formulation is not strictly variational due to the projection of the CCSD amplitudes on the reference state and due to the perturbative nature of the (T) contribution. Nevertheless, in the end both approaches should result (at some point in the future) at the same total exact energy, and it is interesting to check how far the community has come.

There were four DFAs (PWPB95, mPWB1K, mPW1B95, PW6B95) that showed SCF problems during one or more of the optimizations and frequency calculations, which in all cases involved the $^2[FAlO_2]^{\bullet+}$ system. Additionally, mPW1B95 showed problems as well for $[FAlO_2]^0$ and $[FAl(\mu\text{-}O)_2AlF]^0$. These problems were likely caused by the well known numerical instability of the B95 correlation functional,[22] which was solved by increasing the integration grid to (770,123) for the singlet systems. Further modifications were needed for the unrestricted $^2[FAlO_2]^{\bullet+}$ system: changing the SCF procedure to EDIIS and loosening the convergence criteria for energy (10^{-7} Hartree) and density (10^{-5} atomic units) solved the issues there as well.

The mean absolute deviation (MAD) from the coupled cluster reference data for *all* bonds (Table S1) is smallest for the B97-3c composite functional (MAD value 0.0056 Å), followed by MS1/MS2 metagga and the r2SCAN-3c composite functionals (MAD values 0.0064-0.0067 Å), followed by

TPSS (0.0079 Å), the MGGA-hybrid TPSSh (0.0092 Å), revised TPSS (0.0092 Å) and the B97-D2 GGA (0.0094 Å). The best hybrid functional is B3LYP with a MAD value of 0.0118 Å, TMHF the best local hybrid function (0.0156 Å), RC04 is the best LDA functional (0.0169 Å), HSE06 the best range-separated hybrid functional (0.0234 Å), ωLH23tb the best range-separated local hybrid functional (0.0263 Å), and B2PLYP the best double-hybrid functional (0.0357 Å). The lower end of the table is filled with more exotic functionals like revSCAN0 or MVSh, but also includes double-hybrid functionals like DSD-PBEP86 (0.0484 Å) or DSD-BLYP (0.0497 Å).

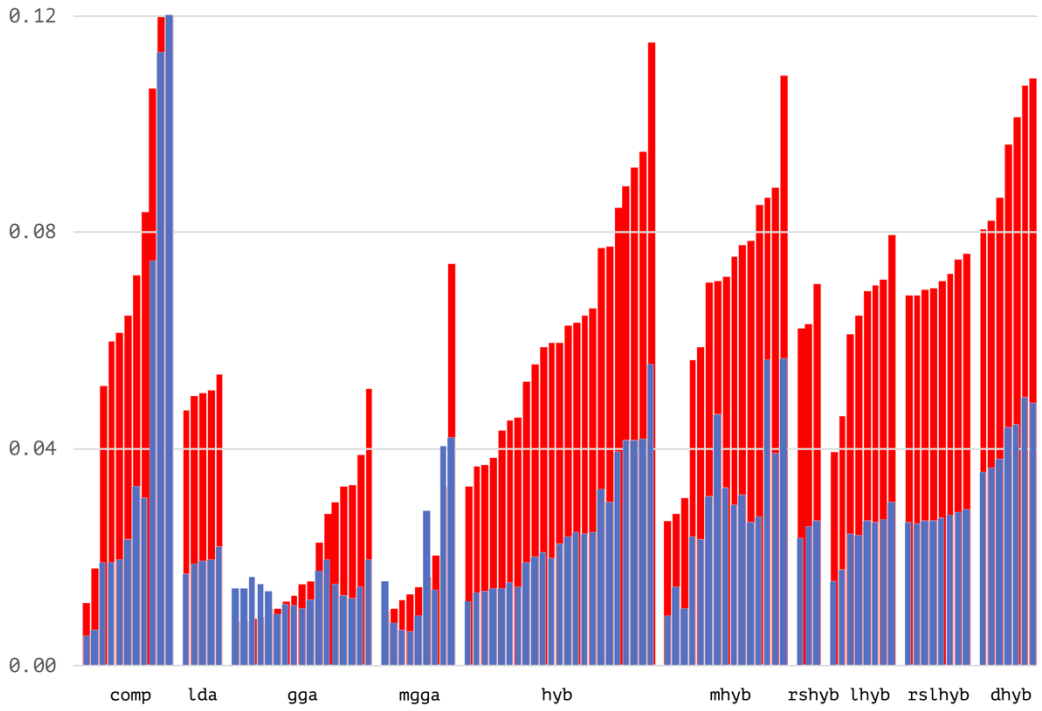

Figure 1. Mean absolute deviations (Å) of all bonds (blue, Table S1) and peroxo/superoxo-bonds alone (red, Table S2) for the 100 density functionals compared to the CCSD(T)/aug-cc-pVQZ reference data. Shown from left to right are the classes of composites, LDA, GGA, MGGA, hybrid, MGGA-hybrid, range-separated hybrid, local hybrid, range-separated local hybrid and double hybrid.

If we now specifically focus on the peroxo/superoxo O-O bonds alone (Table S2, Figure 1), a different picture emerges. TCA, revTCA, RPBE and revPBE are suddenly the best (0.0082-0.0090 Å), followed by PKZB (0.0099 Å), TPSS (0.0105 Å), the Chachiyo and B97-D GGA (0.0106 Å) and B97-3c (0.0116 Å). The best MGGA-hybrid, hybrid, local hybrid, LDA, range-separated hybrid and range-separated local hybrid functionals are again TPSSh, B3LYP, TMHF, RC04, HSE06, and ωLH23tb but with MAD values (0.0267 Å, 0.0330 Å, 0.0396 Å, 0.0472 Å, 0.0623 Å, and 0.0685 Å, respectively) that are more than twice as large as for all bonds. The same holds for B2PLYP, which remains the best-performing double-hybrid functional, but with a MAD value for the peroxo/superoxo bonds of 0.0806 Å. These problems for describing peroxo bonds is observed for many DFAs (see Figure 1).

Most of the density functionals are able to predict well the angles (Table S3), with MAD values of less than 1°, but now with other best-performing functionals for most of the classes: BLYP for GGAs (MAD 0.213°), M06-L for MGGAs (MAD 0.278°), r2SCAN-3c the best composite (MAD 0.302°); B3LYP and TMHF remain best hybrid and local hybrid functional (MAD 0.363° and 0.417°, respectively), MS2h is the best MGGA-hybrid functional (MAD 0.383°), CAM-B3LYP the best range-separated hybrid functional (MAD 0.687°), RC04 best LDA functional (MAD 0.705°), ωLH23tp the best range-separated local hybrid (MAD 0.757°) and PTPSS the best double hybrid (MAD 0.851°).

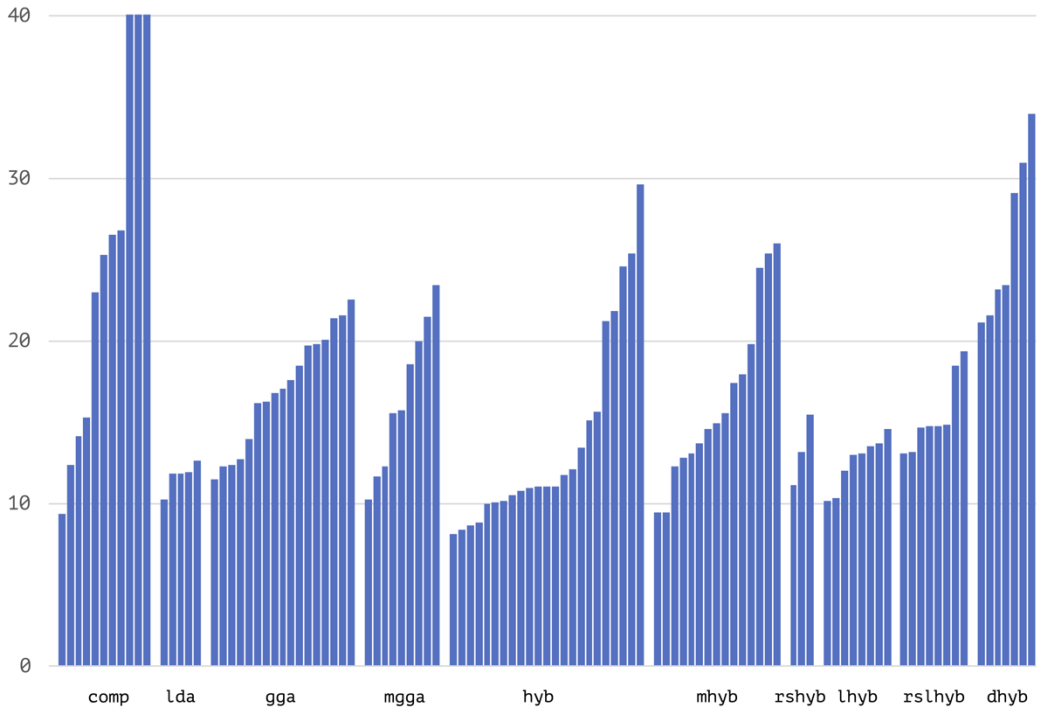

Figure 2. Mean absolute deviations (cm^{-1}) of vibrational frequencies for the 100 density functionals compared to the CCSD(T)/aug-cc-pVQZ reference data. Shown from left to right are the classes of composites, LDA, GGA, MGGA, hybrid, MGGA-hybrid, range-separated hybrid, local hybrid, range-separated local hybrid and double hybrid.

The picture changes again completely when looking at the vibrational frequencies (Table S4, Figure 2). Note that the DFT frequencies were computed at the CCSD(T) geometries; this allows to separate clearly the effect of accuracy for geometries (Tables S1-S3) from the accuracy for frequencies (Table S4). Here the hybrid functionals in all the different guises are observed at the upper half of the list, with the O3LYP hybrid functional performing best (MAD 8.1 cm^{-1}), followed closely by B97 (8.4 cm^{-1}), and B97-1 (8.7 cm^{-1}). The best composite is again r2SCAN-3c (9.4 cm^{-1}). The best MGGA-hybrid functional is now TPSSh (MAD 9.5 cm^{-1}), TMHF is the best local hybrid again (MAD 10.1 cm^{-1}), M06-L is the best metagga functional (MAD 10.2 cm^{-1}), RC04 the best LDA functional (10.3 cm^{-1}), HSE06 the best range-separated hybrid functional (MAD 11.1

cm^{-1}), OPBE the best GGA functional (MAD 11.5 cm^{-1}), ωLH23tde the best range-separated local hybrid (MAD 13.1 cm^{-1}), and PWPB95 the best double-hybrid functional (MAD 21.2 cm^{-1}). Most of the list of 100 DFAs show MAD values for the vibrational frequencies that remain below 20 cm^{-1}, and 68 are within 10 cm^{-1} from the best performing one.

Finally, out of curiosity we also checked how close are the DFA electronic energies to the cc-cf coupled cluster reference values. Again, we mention that these reference energies are not exactly variational, but we expect a very good performance. The double-hybrid, local hybrid and composite functionals are among the best ones for this, corresponding to thirteen of the top fifteen. Surprisingly, the three density functionals that come closest to coupled cluster are not among the top ones for the other four properties. The PKZB metagga functional has a MAD value from the cc-cf values of only 0.3 eV, followed by the SG4 GGA (MAD 1.2 eV), the DSD-BLYP (MAD 2.3 eV) and B2GPPLYP (MAD 3.2 eV) double hybrid functionals. The latter two are among the poorest 15 functionals for the bonds, angles and frequencies, while for PKZB the situation is mixed: it is among the top 35 for angles and all bonds, among the top 5 for the (su)peroxo bonds, but among the lowest 20 for frequencies. For the rest there does not seem to be a clear trend between the class of functional, and the performance for these electronic energies (except for the double-hybrids, *vide supra*). For instance, the BLYP GGA (MAD 23.3 eV) is closer to coupled cluster than B3LYP (MAD 24.0 eV), but even closer are range-separated CAM-B3LYP (MAD 21.5 eV) and B1LYP (MAD 21.5 eV). However, the PBE and OPBE GGA functionals are even better, with MAD values of 12.0 eV and 17.7 eV, respectively; the corresponding PBE1PBE hybrid functional is almost as close as PBE with a MAD value of 12.1 eV. The revPBE (MAD 19.4 eV), RPBE (MAD 22.0 eV) and PBEsol (MAD 26.2 eV) are significantly farther away from the coupled cluster electronic energies than the non-empirical PBE.

The comparison of the LDA functionals adds some interesting results. The RC04 PW92 representation is for most properties the most accurate, with the PW92 and VWN5 of Vosko-Wilk-Nusair following, and the VWN-RPA representation lagging both of them. However, this is

reversed in the comparison of the electronic energies, where VWN-RPA gives a MAD value of 36.2 eV, while VWN5 and PW92 show drastically larger differences with 59.2 eV and 59.6 eV, respectively. The RC04 is now farthest with a difference of 76.1 eV.

Overall assessment. Based on the MAD values for the five different properties (Table S1-S5), we also made an average assessment of the different density functionals. This was done by taking for each DFA the product of the MAD values for the different properties (PROD, shown in Table S6). The top 10 of this final list consists only of composite, GGA and MGGA functionals, with PKZB at the top (PROD 0.0006 $Å^{2}\cdot°\cdot cm^{-1}\cdot eV$), followed closely by SG4 (PROD 0.0041 $Å^{2}\cdot°\cdot cm^{-1}\cdot eV$), and B97-3c (PROD 0.0044 $Å^{2}\cdot°\cdot cm^{-1}\cdot eV$). The best functionals for each class of DFAs are: PKZB (MGGA, PROD 0.0006 $Å^{2}\cdot°\cdot cm^{-1}\cdot eV$), SG4 (GGA, PROD 0.0041 $Å^{2}\cdot°\cdot cm^{-1}\cdot eV$), B97-3c (composite, PROD 0.0044 $Å^{2}\cdot°\cdot cm^{-1}\cdot eV$), TPSSh (MGGA-hybrid, PROD 0.0219 $Å^{2}\cdot°\cdot cm^{-1}\cdot eV$), rev-B3LYP (hybrid, PROD 0.0324 $Å^{2}\cdot°\cdot cm^{-1}\cdot eV$), TMHF (local hybrid, PROD 0.1171 $Å^{2}\cdot°\cdot cm^{-1}\cdot eV$), HSE06 (range-separated hybrid, PROD 0.1544 $Å^{2}\cdot°\cdot cm^{-1}\cdot eV$), ωLH23te (range-separated local hybrid, PROD 0.2496 $Å^{2}\cdot°\cdot cm^{-1}\cdot eV$), PTPSS (double hybrid, PROD 0.3302 $Å^{2}\cdot°\cdot cm^{-1}\cdot eV$) and VWN(RPA) (LDA, 0.3932 $Å^{2}\cdot°\cdot cm^{-1}\cdot eV$).

The average PROD value for all 100 functionals is rather high (11.672 $Å^{2}\cdot°\cdot cm^{-1}\cdot eV$), but this is distorted by the two highest values for BHandH (9.017 $Å^{2}\cdot°\cdot cm^{-1}\cdot eV$) and HF-3c (290.469 $Å^{2}\cdot°\cdot cm^{-1}\cdot eV$). Instead, by taking the product of the averages for each of the five properties (Table 4), one obtains a PROD value of only 0.556 $Å^{2}\cdot°\cdot cm^{-1}\cdot eV$, which is a more appropriate overall measure.

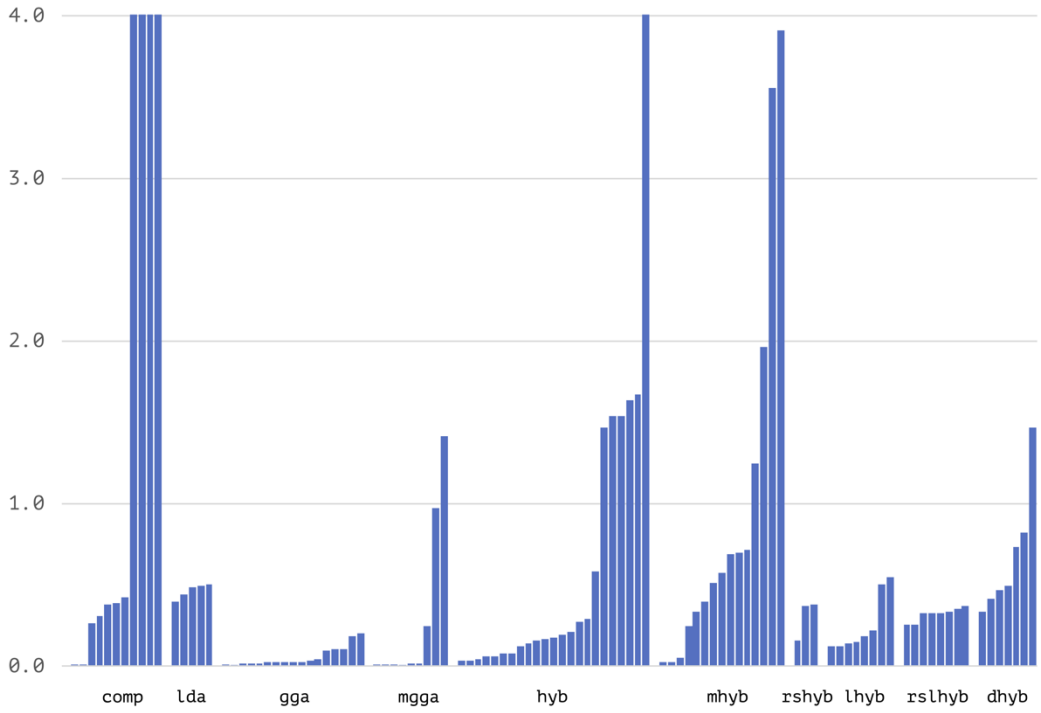

Figure 3. Overall assessment ($Å^{2}\cdot°\cdot cm^{-1}\cdot eV$) for the 100 density functionals compared to the CCSD(T)/aug-cc-pVQZ reference data. Shown from left to right are the classes of composites, LDA, GGA, MGGA, hybrid, MGGA-hybrid, range-separated hybrid, local hybrid, range-separated local hybrid and double hybrid.

Table 4. Statistics for deviations by DFAs (Table S1-S6) from CCSD(T)/aug-cc-pVQZ data

	min. MAD	max. MAD	average
all bonds (Å)	0.0056	0.1303	0.0265
dioxygen bonds (Å)	0.0083	0.2674	0.0591
angles (°)	0.2125	3.1014	0.7677
frequencies (cm^{-1})	8.133	262.430	20.956
electronic energies (eV)	0.288	117.273	22.073
product	0.0006	290.4687	11.6719

Balance of exchange and correlation parts. For the dioxygen bonds, there is not a clear trend on the importance of either exchange or correlation. For instance, when comparing the deviations for O_2 distances by a variety of functionals based on the PBEc and Becke88x functionals, we observe a clear and large effect of the exchange part. Whereas PBE itself slightly underestimates the O_2 bond lengths (as estimated by inspecting the MD value in Table 5), the revPBE and RPBE functionals largely improve upon this. These latter two DFAs modify the exchange part of PBE. Likewise, OPBE, S12g and PBE1PBE, which modify the PBEx in different ways, show a systematic underestimation of the O_2 bonds by 0.030 Å (S12g) to 0.066 Å (PBE1PBE). This appears to indicate a major effect by the choice of exchange functional. However, by comparing the results of combining Becke88 exchange with different correlation functionals, similar effects are seen (ranging from -0.006 to +0.023 Å). Hence, both parts of the DFA formulation play an important role.

Table 5. Statistics[a] (Å) for deviations for O_2 bonds by DFAs based on PBEc and Becke88 parts

DFA	X	C	MAD	MD	Max	Min
PBE	PBEx	PBEc	0.0157	-0.0104	0.0106	-0.0221
revPBE	revPBEx	PBEc	0.0091	-0.0003	0.0172	-0.0100
RPBE	RPBEx	PBEc	0.0087	0.0030	0.0195	-0.0062
OPBE	Optx	PBEc	0.0511	-0.0511	-0.0176	-0.0699
S12g	S12gX	PBEc	0.0302	-0.0302	-0.0066	-0.0419
PBE1PBE	25% HFX + 75% PBEx	PBEc	0.0659	-0.0659	-0.0330	-0.0856
BP86(PZ81)	Becke88	P86 + PZ81	0.0119	-0.0042	0.0153	-0.0154
BP86(VWN)	Becke88	P86 + VWN	0.0129	-0.0059	0.0140	-0.0172
BLYP	Becke88	LYPc	0.0229	0.0229	0.0325	0.0169

a) MAD: Mean Absolute Deviation, MD: Mean Deviation, Max: Maximum deviation, Min: Minimum Deviation

Conclusions

A new set of small dioxygen compounds is presented, for which high-level ab initio calculations were feasible at the CCSD(T)/aug-cc-pVQZ level. The resulting data could be used as reference in the development of new density functionals, or used to benchmark existing density functionals. The latter is done here, for a total of 100 density functionals coming from ten classes (LDA, GGA, MGGA, hybrid, MGGA hybrid, range-separated hybrid, local hybrid, range-separated local hybrid, double hybrid and composites). In general, the density functionals are remarkably accurate for bonds and angles, with average deviations of 0.027 Å for *all* bonds, 0.77° for angles; dioxygen bonds are more difficult to get right, with an average deviation from the coupled cluster of 0.058 Å, more than twice as large as the deviation for all bonds. The cause for this is difficult to pinpoint onto ingredients of DFAs or specific chemical bonding patterns. The frequencies from coupled cluster calculations are off by ca. 10-20 cm^{-1}, where it should be noted that the well-known Hartree-Fock instability can significantly affect the frequency values for open-shell systems. Finally, there is still a long way to go before density functional theory and coupled cluster theory converge to the same exact energy: for the systems studied here on average a deviation of 22.9 eV was observed.

Computational details

Coupled cluster: All CCSD(T) calculations with the aug-cc-pVQZ[23,24] and aug-cc-pV(Q+d)Z[16] basis set were carried out with CFOUR (version 2.0/2.1),[25,26] based on analytical gradients and Hessians,[27–29] in parallel where needed,[30] using unrestricted Hartree-Fock for open-shell systems. Note that a bugfix (Dec. 2021, see SI) was needed for being able to run in parallel with unrestricted coupled cluster protocols. Basis sets not available in standard CFOUR (e.g. def2-TZVPD or aug-cc-pV(Q+d)Z) were obtained from the basis set exchange.[31] The frozen core approach was used within the solving of the coupled cluster equations. The geometry optimization typically had SCF and coupled-cluster convergence criteria of $1.0 \cdot 10^{-10}$, geometry converge of $1.0 \cdot 10^{-8}$ atomic units,

leading to electronic energies accurate to at least $1.0 \cdot 10^{-8}$ Hartree. The two-electron integrals were in all cases treated with the AOBASIS formalism to reduce disk space, in conjunction with the ECC program (with conventional UCCSD(T) for complex **2**). Goodson's continued fraction approach[21] was used to estimate a closer approximation of the full-CI electronic energy (cc-cf), based on the CCSD and CCSD(T) energies. The continued fraction is an extrapolation technique with a characteristic form:

$$a_1/(1 + a_2/(1 + a_3/(1+\ldots)))$$

For a coupled cluster sequence, the electronic energy can be expressed as:

$$E_{cc} = \delta_1 + \delta_2 + \delta_3$$

$$\delta_1 = E_{scf} \;\; ; \;\; \delta_2 = E_{CCSD} - E_{scf} \;\; ; \;\; \delta_3 = E_{CCSD(T)} - E_{CCSD}$$

Since $\delta_1 \gg \delta_2 + \delta_3$, and under the valid assumption that $\delta_2 \gg \delta_3$ this can be rewritten as the continued fraction extrapolated energy value:

$$E_{cc,cf} = \frac{\delta_1}{1 - \frac{\delta_2/\delta_1}{1 - \delta_3/\delta_2}}$$

As shown by Schröder and co-workers,[32] Goodson's approach does not directly extrapolate towards the full-CI limit, but rather to the next excitation level in the coupled cluster series, which in this case would be CCSDTQ.

Additional CCSD(T) calculations using the same basis set and R(O)KS orbitals obtained by the PBE functional were performed with the MOLPRO program package (Version 2022.2).[33,34] All calculations employed the spin-unrestricted CCSD(T) routines (UCCSD(T)) to correctly handle the KS orbitals.

At the same level, also CASPT2 calculations were performed using a CASSCF wave function based on an active space containing the 2s and 2p orbitals of both O atoms. The initial guess for the active space was obtained using the atomic valance active space (AVAS) procedure[35] based on R(O)HF orbitals and both CASSCF and CASPT2 employed density fitting.[36]

Density functional theory: Most density functional calculations were calculated with the psi4 program (release 1.6.1, the composite results were obtained with version 1.9).[37–39] For optimizations, the most tight criteria available in the program were used (*gradient max 2.0·10^{-6} a.u., RMS force 1.0·10^{-6} a.u., max displacement 6.0·10^{-6} a.u., rms displacement 4.0·10^{-6} a.u.*), with typically a grid based on 590 spherical points and 99 radial points. The doublet states (**2**) were treated using the unrestricted Kohn-Sham formalism. Similar to coupled cluster, the DFA calculations were performed in the gas-phase, without relativistic corrections, and using the aug-cc-pVQZ basis set (using RI/DF basis sets, AUG-CC-PVQZ AUX). Some of the results for density functional approximations were obtained through the LibXC[40] library, either the one available directly in psi4, or compiled separately and linked to it. We have studied DFAs of different classes: local density approximation (VWN(RPA),[41] VWN5[41] and PW92[42]), generalized gradient approximations (B97-d,[43] BLYP,[44,45] BP86-PZ81,[44,46,47] BP86-VWN,[41,44,46] OPBE,[48–50] PBE,[50] PBEsol,[51] PW91,[52] revPBE,[53] RPBE,[54] S12g,[55] SOGGA,[56] XLYP[57]), meta-GGA approximations (M06-L,[58] MS1,[59] MS2,[59] MVS,[60] PKZB,[61] revSCAN,[62] revTPSS,[63] SCAN,[64] TPSS[65]), hybrid functionals (B1LYP,[66] B1PW91,[66] B3LYP,[44,45,67] B3PW91,[44,52,68] B97,[69] B97-1,[70] B97-2,[71] B97-3,[72] B97-k,[73] BHandH,[44,68] BHandHLYP,[44,45,68] HJS-PBE,[74] LDA1LDA,[75] mPW1K,[76] mPW1PW,[77] mPWB1K,[78] O3LYP,[45,49,79] PBE1PBE,[50,80] revB3LYP,[81] revPBE1PBE,[50,53,80] SOGGA11-X,[82] X3LYP[57]), hybrid meta-GGA (BB1K,[83] BMK,[73] M06,[84] M06-2X,[84] M08-HX,[85] M11,[86] MS2h,[59] MVSh,[60] MN15,[87] mPW1B95,[78] PW6B95,[88] revSCAN1SCAN,[62] revTPSSh,[89] SCAN1SCAN,[90] TPSSh[65,91]), range-separated hybrids (CAM-B3LYP,[92] HSE06,[93–95] ωB97X-D[96,97]), double hybrids (B2GPPLYP,[98] B2PLYP,[99] DSD-BLYP,[100] DSD-PBEP86,[100] PBE1PBE-DH,[101] PTPSS,[102] PWPB95[102]) and composite methods (HF-3c,[103,104] PBEh-3c[103,104], B97-3c,[105] r2SCAN-3c,[106] ωB97X-3c[107]). Note that ωB97X-3c standard uses a vDZP basis set, which includes an Effective Core Potential (ECP); as a result the electronic energies are completely off (see Supporting Information). Therefore, similar to PBEh-3c the def2-mSVP basis has been used with ωB97X-3c; this change hardly

affects angles and frequencies, slightly improves bonds, and has a major effect only on the electronic energy MAD (see SI).

Additional density functional calculations were performed using a development version of the TURBOMOLE program package based on version 7.8.[108,109] The calculations employed basis sets and convergence criteria identical to those above and were performed using the "reference" grid settings based on 1202 spherical points and 90 radial points (95 for Al). Using TURBOMOLE, we evaluated functionals from additional classes: local hybrids (LH20t,[110] LH23pt,[111] TMHF,[112] TMHF-3P,[112] LHJ-HF,[112] LHJ-HFcal,[112] scLH22t,[113] scLH23t-mBR[114]) and range-separated local hybrids (ωLH22t,[115] ωLH23td,[116] ωLH23te,[116] ωLH23tde,[116] ωLH23tp,[116] ωLH23tdp,[116] ωLH23tb,[116] ωLH23tdb[116]).

Acknowledgments

The authors would like to thank AEI/MCIN (CTQ2017-87392-P, PID2020-114548GB-I00) and GenCat (2021 SGR 00487) for funding.

References

(1) Cramer, C. J.; Tolman, W. B.; Theopold, K. H.; Rheingold, A. L. Variable Character of O-O and M-O Bonding in Side-on (n. *Proc. Natl. Acad. Sci. USA* **2003**, *100*, 3635–3640. https://doi.org/10.1073.

(2) Swart, M. A Change in the Oxidation State of Iron: Scandium Is Not Innocent. *Chem. Commun.* **2013**, *49* (59). https://doi.org/10.1039/c3cc42200c.

(3) Deeth, R. J.; Fey, N. The Performance of Nonhybrid Density Functionals for Calculating the Structures and Spin States of Fe(II) and Fe(III) Complexes. *J. Comput. Chem.* **2004**, *25*, 1840–1848.

(4) Weymuth, T.; Couzijn, E. P. A.; Chen, P.; Reiher, M. New Benchmark Set of Transition-Metal Coordination Reactions for the Assessment of Density Functionals. *J. Chem. Theory Comput.* **2014**, *10* (8), 3092–3103. https://doi.org/10.1021/ct500248h.

(5) Houghton, B. J.; Deeth, R. J. Spin-State Energetics of FeII Complexes - The Continuing Voyage Through the Density Functional Minefield. *Eur. J. Inorg. Chem.* **2014**, *2014*, 4573–4580. https://doi.org/10.1002/ejic.201402253.

(6) Reimann, M.; Kaupp, M. Spin-State Splittings in 3d Transition-Metal Complexes Revisited: Benchmarking Approximate Methods for Adiabatic Spin-State Energy Differences in Fe(II) Complexes. *J. Chem. Theory Comput.* **2022**, *18* (12), 7442–7456. https://doi.org/10.1021/acs.jctc.2c00924.

(7) Reimann, M.; Kaupp, M. Spin-State Splittings in 3d Transition-Metal Complexes Revisited: Toward a Reliable Theory Benchmark. *J. Chem. Theory Comput.* **2023**, *19* (1), 97–108. https://doi.org/10.1021/acs.jctc.2c00925.

(8) Vennelakanti, V.; Taylor, M. G.; Nandy, A.; Duan, C.; Kulik, H. J. Assessing the Performance of Approximate Density Functional Theory on 95 Experimentally Characterized Fe(II) Spin Crossover Complexes. *J. Chem. Phys.* **2023**, *159* (2), 024120. https://doi.org/10.1063/5.0157187.

(9) Koch, W.; Holthausen, M. C. *A Chemist's Guide to Density Functional Theory*; Wiley-VCH, 2000.

(10) Cramer, C. J.; Truhlar, D. G. Density Functional Theory for Transition Metals and Transition Metal Chemistry. *Phys. Chem. Chem. Phys.* **2009**, *11*, 10757–10816.

(11) Bursch, M.; Mewes, J.-M.; Hansen, A.; Grimme, S. Best-Practice DFT Protocols for Basic Molecular Computational Chemistry**. *Angew. Chem. Int. Ed.* **2022**, *61* (42), e202205735. https://doi.org/10.1002/anie.202205735.

(12) Bahlo, J.; Himmel, H.-J.; Schnöckel, H. The First Dectection of Peroxo and Bis-Superoxo Complexes of Aluminum: FAlO2 and FAlO4. *Angew. Chem. Int. Ed.* **2001**, *40* (24), 4696–4700. https://doi.org/10.1002/1521-3773(20011217)40:24<4696::AID-ANIE4696>3.0.CO;2-W.

(13) Bahlo, J.; Himmel, H.-J.; Schnöckel, H. Photolytic Reactions of Subvalent Aluminum(I) Halides in the Presence of Dioxygen: Generation and Characterization of the Peroxo Species XAlO2 and XAl(μ-O)2AlX (X = F, Cl, Br). *Inorg. Chem.* **2002**, *41* (10), 2678–2689. https://doi.org/10.1021/ic011313d.

(14) Tremblay, B.; Roy, P.; Manceron, L.; Alikhani, M. E.; Roy, D. Vibrational Spectrum and Structure of Silicon Trioxide SiO3: A Matrix Isolation Infrared and Density Functional Theory Study. *J. Chem. Phys.* **1996**, *104* (8), 2773–2781. https://doi.org/10.1063/1.471100.

(15) Helgaker, T.; Jørgensen, P.; Olsen, J. *Molecular Electronic-Structure Theory*; Wiley, 2000.

(16) Dunning, T. H., Jr.; Peterson, K. A.; Wilson, A. K. Gaussian Basis Sets for Use in Correlated Molecular Calculations. X. The Atoms Aluminum through Argon Revisited. *J. Chem. Phys.* **2001**, *114* (21), 9244–9253. https://doi.org/10.1063/1.1367373.

(17) Crawford, T. D.; Stanton, J. F.; Allen, W. D.; Schaefer, H. F., III. Hartree–Fock Orbital Instability Envelopes in Highly Correlated Single-Reference Wave Functions. *J. Chem. Phys.* **1997**, *107* (24), 10626–10632. https://doi.org/10.1063/1.474178.

(18) Cordero, B.; Gómez, V.; Platero-Prats, A. E.; Revés, M.; Echeverría, J.; Cremades, E.; Barragán, F.; Alvarez, S. Covalent Radii Revisited. *Dalton Trans.* **2008**, No. 21, 2832–2838. https://doi.org/10.1039/B801115J.

(19) Hammerl, A.; Welch, B. J.; Schwerdtfeger, P. F2Al(μ-H2:H2-O2)AlF2: An Unusual, Stable Aluminum Peroxo Compound. *Inorg. Chem.* **2004**, *43* (4), 1436–1440. https://doi.org/10.1021/ic035014v.

(20) Bahlo, J.; Himmel, H.-J.; Schnöckel, H. Characterization of the Side-On Coordinated Bissuperoxo Complexes of Aluminum FAl(O2)2, ClAl(O2)2, and BrAl(O2)2 with Triplet Electronic Ground States: A Combined Matrix IR and Quantum Chemical Study. *Inorg. Chem.* **2002**, *41* (17), 4488–4495. https://doi.org/10.1021/ic020208g.

(21) Goodson, D. Z. Extrapolating the Coupled−cluster Sequence toward the Full Configuration−interaction Limit. *J. Chem. Phys.* **2002**, *116*, 6948–6956. https://doi.org/10.1063/1.1462620.

(22) Zhao, Y.; Truhlar, D. G. Benchmark Databases for Nonbonded Interactions and Their Use To Test Density Functional Theory. *J. Chem. Theory Comput.* **2005**, *1* (3), 415–432. https://doi.org/10.1021/ct049851d.

(23) Kendall, R. A.; Jr, T. H. D.; Harrison, R. J. Electron Affinities of the First-row Atoms Revisited. Systematic Basis Sets and Wave Functions. *J. Chem. Phys.* **1992**, *96*, 6796–6808.

(24) Woon, D. E.; Dunning, T. H., Jr. Gaussian Basis Sets for Use in Correlated Molecular Calculations. III. The Atoms Aluminum through Argon. *J. Chem. Phys.* **1993**, *98* (2), 1358–1371. https://doi.org/10.1063/1.464303.

(25) Stanton, J. F.; Gauss, J.; Cheng, L.; Harding, M. E.; Matthews, D. A.; Szalay, P. G. CFOUR, Coupled-Cluster Techniques for Computational Chemistry, a Quantum-Chemical Program Package.

(26) Matthews, D. A.; Cheng, L.; Harding, M. E.; Lipparini, F.; Stopkowicz, S.; Jagau, T.-C.; Szalay, P. G.; Gauss, J.; Stanton, J. F. Coupled-Cluster Techniques for Computational Chemistry: The CFOUR Program Package. *J. Chem. Phys.* **2020**, *152* (21), 214108. https://doi.org/10.1063/5.0004837.

(27) Watts, J. D.; Gauss, J.; Bartlett, R. J. Open-Shell Analytical Energy Gradients for Triple Excitation Many-Body, Coupled-Cluster Methods: MBPT(4), CCSD+T(CCSD), CCSD(T),and QCISD(T). *Chem. Phys. Lett.* **1992**, *200* (1), 1–7. https://doi.org/10.1016/0009-2614(92)87036-O.

(28) Gauss, J.; Stanton, J. F. Analytic CCSD(T) Second Derivatives. *Chem. Phys. Lett.* **1997**, *276* (1), 70–77. https://doi.org/10.1016/S0009-2614(97)88036-0.

(29) Szalay, P. G.; Gauss, J.; Stanton, J. F. Analytic UHF-CCSD(T) Second Derivatives: Implementation and Application to the Calculation of the Vibration-Rotation Interaction Constants of NCO and NCS. *Theor. Chem. Acc.* **1998**, *100* (1), 5–11. https://doi.org/10.1007/s002140050360.

(30) Harding, M. E.; Metzroth, T.; Gauss, J. Parallel Calculation of CCSD and CCSD(T) Analytic First and Second Derivatives. *J. Chem. Theory Comput.* **2008**, *4*, 64–74. https://doi.org/10.1021/ct700152c.

(31) Pritchard, B. P.; Altarawy, D.; Didier, B.; Gibson, T. D.; Windus, T. L. New Basis Set Exchange: An Open, Up-to-Date Resource for the Molecular Sciences Community. *J. Chem. Inf. Model.* **2019**, *59* (11), 4814–4820. https://doi.org/10.1021/acs.jcim.9b00725.

(32) Schröder, B.; Sebald, P.; Stein, C.; Weser, O.; Botschwina, P. Challenging High-Level Ab Initio Rovibrational Spectroscopy: The Nitrous Oxide Molecule. **2015**, *229* (10–12), 1663–1690. https://doi.org/10.1515/zpch-2015-0622.

(33) Werner, H.-J.; Knowles, P. J.; Manby, F. R.; Black, J. A.; Doll, K.; Heßelmann, A.; Kats, D.; Köhn, A.; Korona, T.; Kreplin, D. A.; Ma, Q.; Miller, T. F., III; Mitrushchenkov, A.; Peterson, K. A.; Polyak, I.; Rauhut, G.; Sibaev, M. The Molpro Quantum Chemistry Package. *J. Chem. Phys.* **2020**, *152* (14), 144107. https://doi.org/10.1063/5.0005081.

(34) H.-J. Werner, P. J. Knowles, P. Celani, W. Györffy, A. Hesselmann, D. Kats, G. Knizia, A. Köhn, T. Korona, D. Kreplin, R. Lindh, Q. Ma, F. R. Manby, A. Mitrushenkov, G. Rauhut, M. Schütz, K. R. Shamasundar, T. B. Adler, R. D. Amos, J. Baker, S. J. Bennie, A.

Bernhardsson, A. Berning, J. A. Black, P. J. Bygrave, R. Cimiraglia, D. L. Cooper, D. Coughtrie, M. J. O. Deegan, A. J. Dobbyn, K. Doll and M. Dornbach, F. Eckert, S. Erfort, E. Goll, C. Hampel, G. Hetzer, J. G. Hill, M. Hodges and T. Hrenar, G. Jansen, C. Köppl, C. Kollmar, S. J. R. Lee, Y. Liu, A. W. Lloyd, R. A. Mata, A. J. May, B. Mussard, S. J. McNicholas, W. Meyer, T. F. Miller III, M. E. Mura, A. Nicklass, D. P. O'Neill, P. Palmieri, D. Peng, K. A. Peterson, K. Pflüger, R. Pitzer, I. Polyak, P. Pulay, M. Reiher, J. O. Richardson, J. B. Robinson, B. Schröder, M. Schwilk and T. Shiozaki, M. Sibaev, H. Stoll, A. J. Stone, R. Tarroni, T. Thorsteinsson, J. Toulouse, M. Wang, M. Welborn and B. Ziegler. MOLPRO, Version 2022.2, a Package of Ab Initio Programs. https://www.molpro.net.

(35) Sayfutyarova, E. R.; Sun, Q.; Chan, G. K.-L.; Knizia, G. Automated Construction of Molecular Active Spaces from Atomic Valence Orbitals. *J. Chem. Theory Comput.* **2017**, *13* (9), 4063–4078. https://doi.org/10.1021/acs.jctc.7b00128.

(36) Győrffy, W.; Shiozaki, T.; Knizia, G.; Werner, H.-J. Analytical Energy Gradients for Second-Order Multireference Perturbation Theory Using Density Fitting. *J. Chem. Phys.* **2013**, *138* (10), 104104. https://doi.org/10.1063/1.4793737.

(37) Smith, D. G. A.; Burns, L. A.; Simmonett, A. C.; Parrish, R. M.; Schieber, M. C.; Galvelis, R.; Kraus, P.; Kruse, H.; Di Remigio, R.; Alenaizan, A.; James, A. M.; Lehtola, S.; Misiewicz, J. P.; Scheurer, M.; Shaw, R. A.; Schriber, J. B.; Xie, Y.; Glick, Z. L.; Sirianni, D. A.; O'Brien, J. S.; Waldrop, J. M.; Kumar, A.; Hohenstein, E. G.; Pritchard, B. P.; Brooks, B. R.; Schaefer, H. F., III; Sokolov, A. Yu.; Patkowski, K.; DePrince, A. E., III; Bozkaya, U.; King, R. A.; Evangelista, F. A.; Turney, J. M.; Crawford, T. D.; Sherrill, C. D. PSI4 1.4: Open-Source Software for High-Throughput Quantum Chemistry. *J. Chem. Phys.* **2020**, *152* (18), 184108. https://doi.org/10.1063/5.0006002.

(38) Almlöf, J.; Faegri Jr., K.; Korsell, K. Principles for a Direct SCF Approach to LICAO–MOab-Initio Calculations. *J. Comput. Chem.* **1982**, *3* (3), 385–399. https://doi.org/10.1002/jcc.540030314.

(39) Van Lenthe, J. H.; Zwaans, R.; Van Dam, H. J. J.; Guest, M. F. Starting SCF Calculations by Superposition of Atomic Densities. *J. Comput. Chem.* **2006**, *27* (8), 926–932. https://doi.org/10.1002/jcc.20393.

(40) Lehtola, S.; Steigemann, C.; Oliveira, M. J. T.; Marques, M. A. L. Recent Developments in Libxc — A Comprehensive Library of Functionals for Density Functional Theory. *SoftwareX* **2018**, *7*, 1–5. https://doi.org/10.1016/j.softx.2017.11.002.

(41) Vosko, S. H.; Wilk, L.; Nusair, M. Accurate Spin-Dependent Electron Liquid Correlation Energies for Local Spin-Density Calculations - A Critical Analysis. *Can. J. Phys.* **1980**, *58*, 1200–1211.

(42) Perdew, J. P.; Wang, Y. Accurate And Simple Analytic Representation Of The Electron-Gas Correlation-Energy. *Phys. Rev. B* **1992**, *45* (23), 13244–13249.

(43) Grimme, S. Semiempirical GGA-Type Density Functional Constructed with a Long-Range Dispersion Correction. *J. Comput. Chem.* **2006**, *27*, 1787–1799.

(44) Becke, A. D. Density-Functional Exchange-Energy Approximation with Correct Asymptotic Behavior. *Phys. Rev. A* **1988**, *38*, 3098–3100.

(45) Lee, C.; Yang, W.; Parr, R. G. Development of the Colle-Salvetti Correlation-Energy Formula into a Functional of the Electron Density. *Phys. Rev. B* **1988**, *37* (2), 785–789.

(46) Perdew, J. P. Density-Functional Approximation for the Correlation-Energy of the Inhomogeneous Electron-Gas. *Phys. Rev. B* **1986**, *33*, 7406, 8822-8824. Erratum: Ibid. 34.

(47) Perdew, J. P.; Zunger, A. Self-Interaction Correction to Density-Functional Approximations for Many-Electron Systems. *Phys. Rev. B* **1981**, *23* (10), 5048–5079.

(48) Swart, M.; Ehlers, A. W.; Lammertsma, K. Performance of the OPBE Exchange-Correlation Functional. *Mol. Phys.* **2004**, *102* (23–24). https://doi.org/10.1080/00268970420002750l7.

(49) Handy, N. C.; Cohen, A. J. Left-Right Correlation Energy. *Mol. Phys.* **2001**, *99* (5), 403–412.

(50) Perdew, J. P.; Burke, K.; Ernzerhof, M. Generalized Gradient Approximations Made Simple. *Phys. Rev. Lett.* **1996**, *77*, 3865–3868.

(51) Perdew, J. P.; Ruzsinszky, A.; Csonka, G. I.; Vydrov, O. A.; Scuseria, G. E.; Constantin, L. A.; Zhou, X.; Burke, K. Restoring the Density-Gradient Expansion for Exchange in Solids and Surfaces. *Phys. Rev. Lett.* **2008**, *100*, 136406.

(52) Perdew, J. P.; Chevary, J. A.; Vosko, S. H.; Jackson, K. A.; Pederson, M. R.; Singh, D. J.; Fiolhais, C. Atoms, Molecules, Solids, and Surfaces: Applications of the Generalized Gradient Approximation for Exchange and Correlation. *Phys. Rev. B* **1992**, *46* (11), 6671.

(53) Zhang, Y.; Yang, W. revPBE. *Phys. Rev. Lett.* **1998**, *80*, 890.

(54) Hammer, B.; Hansen, L. B.; Norskov, J. K. RPBE. *Phys. Rev. B* **1999**, *59*, 7413.

(55) Swart, M. A New Family of Hybrid Density Functionals. *Chem. Phys. Lett.* **2013**, *580*. https://doi.org/10.1016/j.cplett.2013.06.045.

(56) Zhao, Y.; Truhlar, D. G. Construction of a Generalized Gradient Approximation by Restoring the Density-Gradient Expansion and Enforcing a Tight Lieb–Oxford Bound. *J. Chem. Phys.* **2008**, *128* (18), 184109. https://doi.org/10.1063/1.2912068.

(57) Xu, X.; III, W. A. G. The X3LYP Extended Density Functional for Accurate Descriptions of Nonbond Interactions, Spin States, and Thermochemical Properties. *Proc. Natl. Acad. Sci. USA* **2004**, *101*, 2673–2677.

(58) Zhao, Y.; Truhlar, D. G. A New Local Density Functional for Main-Group Thermochemistry, Transition Metal Bonding, Thermochemical Kinetics, and Noncovalent Interactions. *J. Chem. Phys.* **2006**, *125*, 194101.

(59) Sun, J.; Haunschild, R.; Xiao, B.; Bulik, I. W.; Scuseria, G. E.; Perdew, J. P. Semilocal and Hybrid Meta-Generalized Gradient Approximations Based on the Understanding of the Kinetic-Energy-Density Dependence. *J. Chem. Phys.* **2013**, *138* (4), 044113. https://doi.org/10.1063/1.4789414.

(60) Sun, J.; Perdew, J. P.; Ruzsinszky, A. Semilocal Density Functional Obeying a Strongly Tightened Bound for Exchange. *Proc. Natl. Acad. Sci. USA* **2015**, *112*, 685–689. https://doi.org/10.1073/pnas.1423145112.

(61) Perdew, J. P.; Kurth, S.; Zupan, A.; Blaha, P. Accurate Density Functional with Correct Formal Properties: A Step beyond the Generalized Gradient Approximation. *Phys. Rev. Lett.* **1999**, *82* (12), 2544–2547.

(62) Mezei, P. D.; Csonka, G. I.; Kállay, M. Simple Modifications of the SCAN Meta-Generalized Gradient Approximation Functional. *J. Chem. Theory Comput.* **2018**, *14* (5), 2469–2479. https://doi.org/10.1021/acs.jctc.8b00072.

(63) Perdew, J.; Ruzsinszky, A.; Csonka, G.; Constantin, L.; Sun, J. Workhorse Semilocal Density Functional for Condensed Matter Physics and Quantum Chemistry. *Phys. Rev. Lett.* **2009**, *103* (2). https://doi.org/10.1103/PhysRevLett.103.026403.

(64) Sun, J.; Ruzsinszky, A.; Perdew, J. P. Strongly Constrained and Appropriately Normed Semilocal Density Functional. *Phys. Rev. Lett.* **2015**, *115*, 36402. https://doi.org/10.1103/PhysRevLett.115.036402.

(65) Tao, J. M.; Perdew, J. P.; Staroverov, V. N.; Scuseria, G. E. Climbing the Density Functional Ladder: Nonempirical Meta- Generalized Gradient Approximation Designed for Molecules and Solids. *Phys. Rev. Lett.* **2003**, *91* (14), 146401.

(66) Adamo, C.; Barone, V. Toward Reliable Adiabatic Connection Models Free from Adjustable Parameters. *Chem. Phys. Lett.* **1997**, *274*, 242–250.

(67) Stephens, P. J.; Devlin, F. J.; Chabalowski, C. F.; Frisch, M. J. Ab Initio Calculation of Vibrational Absorption and Circular Dichroism Spectra Using Density Functional Force Fields. *J. Phys. Chem.* **1994**, *98*, 11623–11627.

(68) Becke, A. D. Density-Functional Thermochemistry. III. The Role of Exact Exchange. *J. Chem. Phys.* **1993**, *98*, 5648–5652.

(69) Becke, A. D. Density-Functional Thermochemistry .5. Systematic Optimization of Exchange-Correlation Functionals. *J. Chem. Phys.* **1997**, *107* (20), 8554–8560.

(70) Hamprecht, F. A.; Cohen, A. J.; Tozer, D. J.; Handy, N. C. Development and Assessment of New Exchange-Correlation Functionals. *J. Chem. Phys.* **1998**, *109* (15), 6264–6271.

(71) Wilson, P. J.; Bradley, T. J.; Tozer, D. J. Hybrid Exchange-Correlation Functional Determined from Thermochemical Data and Ab Initio Potentials. *J. Chem. Phys.* **2001**, *115* (20), 9233–9242. https://doi.org/10.1063/1.1412605.
(72) Keal, T. W.; Tozer, D. J. Semiempirical Hybrid Functional with Improved Performance in an Extensive Chemical Assessment. *J. Chem. Phys.* **2005**, *123* (12), 121103. https://doi.org/10.1063/1.2061227.
(73) Boese, A. D.; Martin, J. M. L. Development of Density Functionals for Thermochemical Kinetics. *J. Chem. Phys.* **2004**, *121* (8), 3405–3416. https://doi.org/10.1063/1.1774975.
(74) Henderson, T. M.; Janesko, B. G.; Scuseria, G. E. Generalized Gradient Approximation Model Exchange Holes for Range-Separated Hybrids. *J. Chem. Phys.* **2008**, *128* (19), 194105. https://doi.org/10.1063/1.2921797.
(75) Rinke, P.; Schleife, A.; Kioupakis, E.; Janotti, A.; Rödl, C.; Bechstedt, F.; Scheffler, M.; Van de Walle, C. G. First-Principles Optical Spectra for F Centers in MgO. *Phys. Rev. Lett.* **2012**, *108* (12), 126404. https://doi.org/10.1103/PhysRevLett.108.126404.
(76) Lynch, B. J.; Fast, P. L.; Harris, M.; Truhlar, D. G. Adiabatic Connection for Kinetics. *J. Phys. Chem. A* **2000**, *104*, 4811–4815.
(77) Adamo, C.; Barone, V. Exchange Functionals with Improved Long-Range Behavior: And Adiabatic Connection Methods without Adjustable Parameters The mPW and mPW1PW Models. *J. Chem. Phys.* **1998**, *108*, 664–675.
(78) Zhao, Y.; Truhlar, D. G. Hybrid Meta Density Functional Theory Methods for Thermochemistry, Thermochemical Kinetics, and Noncovalent Interactions: The MPW1B95 and MPWB1K Models and Comparative Assessments for Hydrogen Bonding and van Der Waals Interactions. *J. Phys. Chem. A* **2004**, *108* (33), 6908–6918. https://doi.org/10.1021/jp048147q.
(79) Cohen, A. J.; Handy, N. C. Dynamic Correlation. *Mol. Phys.* **2001**, *99* (7), 607–615.
(80) Perdew, J. P.; Ernzerhof, M.; Burke, K. Rationale for Mixing Exact Exchange with Density Functional Approximations. *J. Chem. Phys.* **1996**, *105*, 9982–9985.
(81) Lu, L.; Hu, H.; Hou, H.; Wang, B. An Improved B3LYP Method in the Calculation of Organic Thermochemistry and Reactivity. *Comput. Theor. Chem.* **2013**, *1015*, 64–71. https://doi.org/10.1016/j.comptc.2013.04.009.
(82) Peverati, R.; Truhlar, D. G. Communication: A Global Hybrid Generalized Gradient Approximation to the Exchange-Correlation Functional That Satisfies the Second-Order Density-Gradient Constraint and Has Broad Applicability in Chemistry. *J. Chem. Phys.* **2011**, *135* (19), 191102. https://doi.org/10.1063/1.3663871.
(83) Zhao, Y.; Lynch, B. J.; Truhlar, D. G. Development and Assessment of a New Hybrid Density Functional Model for Thermochemical Kinetics. *J. Phys. Chem. A* **2004**, *108* (14), 2715–2719. https://doi.org/10.1021/jp049908s.
(84) Zhao, Y.; Truhlar, D. G. The M06 Suite of Density Functionals for Main Group Thermochemistry, Thermochemical Kinetics, Noncovalent Interactions, Excited States, and Transition Elements: Two New Functionals and Systematic Testing of Four M06-Class Functionals and 12 Other Functionals. *Theor. Chem. Acc.* **2008**, *120*, 215–241.
(85) Zhao, Y.; Truhlar, D. G. Exploring the Limit of Accuracy of the Global Hybrid Meta Density Functional for Main-Group Thermochemistry, Kinetics, and Noncovalent Interactions. *J. Chem. Theory Comput.* **2008**, *4* (11), 1849–1868. https://doi.org/10.1021/ct800246v.
(86) Peverati, R.; Truhlar, D. G. Improving the Accuracy of Hybrid Meta-GGA Density Functionals by Range Separation. *J. Phys. Chem. Lett.* **2011**, *2* (21), 2810–2817. https://doi.org/10.1021/jz201170d.
(87) Yu, H. S.; He, X.; Li, S. L.; Truhlar, D. G. MN15: A Kohn–Sham Global-Hybrid Exchange– Correlation Density Functional with Broad Accuracy for Multi-Reference and Single-Reference Systems and Noncovalent Interactions. *Chem. Sci.* **2016**, *7*, 5032–5051. https://doi.org/10.1039/c6sc00705h.
(88) Zhao, Y.; Truhlar, D. G. Design of Density Functionals That Are Broadly Accurate for Thermochemistry, Thermochemical Kinetics, and Nonbonded Interactions. *J. Phys. Chem. A* **2005**, *109* (25), 5656–5667. https://doi.org/10.1021/jp050536c.
(89) Csonka, G. I.; Perdew, J. P.; Ruzsinszky, A. Global Hybrid Functionals: A Look at the Engine under the Hood. *J. Chem. Theory Comput.* **2010**, *6* (12), 3688–3703. https://doi.org/10.1021/ct100488v.
(90) Hui, K.; Chai, J.-D. SCAN-Based Hybrid and Double-Hybrid Density Functionals from Models without Fitted Parameters. *J. Chem. Phys.* **2016**, *144* (4), 044114. https://doi.org/10.1063/1.4940734.
(91) Staroverov, V. N.; Scuseria, G. E.; Tao, J.; Perdew, J. P. Comparative Assessment of a New Nonempirical Density Functional: Molecules and Hydrogen-Bonded Complexes. *J. Chem. Phys.* **2003**, *119* (23), 12129–12137.
(92) Yanai, T.; Tew, D. P.; Handy, N. C. A New Hybrid Exchange–Correlation Functional Using the Coulomb-Attenuating Method (CAM-B3LYP). *Chem. Phys. Lett.* **2004**, *393*, 51–57. https://doi.org/10.1016/j.cplett.2004.06.011.
(93) Heyd, J.; Scuseria, G. E.; Ernzerhof, M. Hybrid Functionals Based on a Screened Coulomb Potential. *J. Chem. Phys.* **2003**, *118* (18), 8207–8215. https://doi.org/10.1063/1.1564060.
(94) Heyd, J.; Scuseria, G. E.; Ernzerhof, M. Erratum: "Hybrid Functionals Based on a Screened Coulomb Potential" [J. Chem. Phys. 118, 8207 (2003)]. *J. Chem. Phys.* **2006**, *124* (21), 219906. https://doi.org/10.1063/1.2204597.
(95) Krukau, A. V.; Vydrov, O. A.; Izmaylov, A. F.; Scuseria, G. E. Influence of the Exchange Screening Parameter on the Performance of Screened Hybrid Functionals. *J. Chem. Phys.* **2006**, *125* (22), 224106. https://doi.org/10.1063/1.2404663.
(96) Chai, J.-D.; Head-Gordon, M. Long-Range Corrected Hybrid Density Functionals with Damped Atom–Atom Dispersion Corrections. *Phys. Chem. Chem. Phys.* **2008**, *10*, 6615–6620. https://doi.org/10.1039/B810189B.
(97) Chai, J.-D.; Head-Gordon, M. Systematic Optimization of Long-Range Corrected Hybrid Density Functionals. *J. Chem. Phys.* **2008**, *128* (8), 084106. https://doi.org/10.1063/1.2834918.
(98) Karton, A.; Tarnopolsky, A.; Lamère, J.-F.; Schatz, G. C.; Martin, J. M. L. Highly Accurate First-Principles Benchmark Data Sets for the Parametrization and Validation of Density Functional and Other Approximate Methods. Derivation of a Robust, Generally Applicable, Double-Hybrid Functional for Thermochemistry and Thermochemical Kinetics. *J. Phys. Chem. A* **2008**, *112* (50), 12868–12886. https://doi.org/10.1021/jp801805p.
(99) Grimme, S. Semiempirical Hybrid Density Functional with Perturbative Second-Order Correlation. *J. Chem. Phys.* **2006**, *124* (3), 34108. https://doi.org/10.1063/1.2148954.
(100) Kozuch, S.; Martin, J. M. L. Spin-Component-Scaled Double Hybrids: An Extensive Search for the Best Fifth-Rung Functionals Blending DFT and Perturbation Theory. *J. Comput. Chem.* **2013**, *34* (27), 2327–2344. https://doi.org/10.1002/jcc.23391.
(101) Bremond, E.; Adamo, C. Seeking for Parameter-Free Double-Hybrid Functionals: The PBE0-DH Model. *J. Chem. Phys.* **2011**, *135* (2), 24106. https://doi.org/10.1063/1.3604569.
(102) Goerigk, L.; Grimme, S. Efficient and Accurate Double-Hybrid-Meta-GGA Density Functionals—Evaluation with the Extended GMTKN30 Database for General Main Group Thermochemistry, Kinetics, and Noncovalent Interactions. *J. Chem. Theory Comput.* **2011**, *7* (2), 291–309. https://doi.org/10.1021/ct100466k.
(103) Grimme, S.; Antony, J.; Ehrlich, S.; Krieg, H. A Consistent and Accurate Ab Initio Parametrization of Density Functional Dispersion Correction (DFT-D) for the 94 Elements H-Pu. *J. Chem. Phys.* **2010**, *132*, 154104.
(104) Grimme, S.; Ehrlich, S.; Goerigk, L. Effect of the Damping Function in Dispersion Corrected Density Functional Theory. *J. Comput. Chem.* **2011**, *32* (7), 1456–1465. https://doi.org/10.1002/jcc.21759.
(105) Brandenburg, J. G.; Bannwarth, C.; Hansen, A.; Grimme, S. B97-3c: A Revised Low-Cost Variant of the B97-D Density Functional Method. *J. Chem. Phys.* **2018**, *148* (6), 064104. https://doi.org/10.1063/1.5012601.
(106) Grimme, S.; Hansen, A.; Ehlert, S.; Mewes, J.-M. r2SCAN-3c: A "Swiss Army Knife" Composite Electronic-Structure Method. *J. Chem. Phys.* **2021**, *154* (6), 064103. https://doi.org/10.1063/5.0040021.

(107) Müller, M.; Hansen, A.; Grimme, S. ωB97X-3c: A Composite Range-Separated Hybrid DFT Method with a Molecule-Optimized Polarized Valence Double-ζ Basis Set. *J. Chem. Phys.* **2023**, *158* (1), 014103. https://doi.org/10.1063/5.0133026.
(108) Franzke, Y. J.; Holzer, C.; Andersen, J. H.; Begušić, T.; Bruder, F.; Coriani, S.; Della Sala, F.; Fabiano, E.; Fedotov, D. A.; Fürst, S.; Gillhuber, S.; Grotjahn, R.; Kaupp, M.; Kehry, M.; Krstić, M.; Mack, F.; Majumdar, S.; Nguyen, B. D.; Parker, S. M.; Pauly, F.; Pausch, A.; Perlt, E.; Phun, G. S.; Rajabi, A.; Rappoport, D.; Samal, B.; Schrader, T.; Sharma, M.; Tapavicza, E.; Treß, R. S.; Voora, V.; Wodyński, A.; Yu, J. M.; Zerulla, B.; Furche, F.; Hättig, C.; Sierka, M.; Tew, D. P.; Weigend, F. TURBOMOLE: Today and Tomorrow. *J. Chem. Theory Comput.* **2023**, *19* (20), 6859–6890. https://doi.org/10.1021/acs.jctc.3c00347.
(109) TURBOMOLE V7.8 2023, a Development of University of Karlsruhe and Forschungszentrum Karlsruhe GmbH, 1989-2007, TURBOMOLE GmbH, since 2007; Available from Http://Www.Turbomole.Com.
(110) Haasler, M.; Maier, T. M.; Grotjahn, R.; Gückel, S.; Arbuznikov, A. V.; Kaupp, M. A Local Hybrid Functional with Wide Applicability and Good Balance between (De)Localization and Left–Right Correlation. *J. Chem. Theory Comput.* **2020**, *16* (9), 5645–5657. https://doi.org/10.1021/acs.jctc.0c00498.
(111) Haasler, M.; Maier, T. M.; Kaupp, M. Toward a Correct Treatment of Core Properties with Local Hybrid Functionals. *J. Comput. Chem.* **2023**, *44* (32), 2461–2477. https://doi.org/10.1002/jcc.27211.
(112) Holzer, C.; Franzke, Y. J. A Local Hybrid Exchange Functional Approximation from First Principles. *J. Chem. Phys.* **2022**, *157* (3), 034108. https://doi.org/10.1063/5.0100439.
(113) Wodyński, A.; Kaupp, M. Local Hybrid Functional Applicable to Weakly and Strongly Correlated Systems. *J. Chem. Theory Comput.* **2022**, *18* (10), 6111–6123. https://doi.org/10.1021/acs.jctc.2c00795.
(114) Wodyński, A.; Arbuznikov, A. V.; Kaupp, M. Strong-Correlation Density Functionals Made Simple. *J. Chem. Phys.* **2023**, *158* (24), 244117. https://doi.org/10.1063/5.0153463.
(115) Fürst, S.; Haasler, M.; Grotjahn, R.; Kaupp, M. Full Implementation, Optimization, and Evaluation of a Range-Separated Local Hybrid Functional with Wide Accuracy for Ground and Excited States. *J. Chem. Theory Comput.* **2023**, *19* (2), 488–502. https://doi.org/10.1021/acs.jctc.2c00782.
(116) Fürst, S.; Kaupp, M.; Wodyński, A. Range-Separated Local Hybrid Functionals with Small Fractional-Charge and Fractional-Spin Errors: Escaping the Zero-Sum Game of DFT Functionals. *J. Chem. Theory Comput.* **2023**, *19* (23), 8639–8653. https://doi.org/10.1021/acs.jctc.3c00877.